Materials Science & Engineering C 99 (2019) 37–46

Contents lists available at ScienceDirect

Materials Science & Engineering C

journal homepage: www.elsevier.com/locate/msec

Nanocrystalline cellulose decorated quantum dots based tyrosinase biosensor for phenol determination

Fariza Aina Abd Manan[a], Wai Weng Hong[a], Jaafar Abdullah[a,b,*], Nor Azah Yusof[a,b], Ishak Ahmad[c]

[a] Department of Chemistry, Faculty of Science, Universiti Putra Malaysia, 43400 UPM Serdang, Selangor D.E., Malaysia
[b] Institute of Advanced Technology, Universiti Putra Malaysia, 43400 UPM Serdang, Selangor D.E., Malaysia
[c] School of Chemical Sciences and Food Technology, Faculty of Sciences and Technology, Universiti Kebangsaan Malaysia, 43600 Bangi, Selangor D.E., Malaysia

ARTICLE INFO

Keywords:
Nanocrystalline cellulose
Biosensor
Tyrosinase
Electrochemical
Quantum dots

ABSTRACT

Novel biosensor architecture based on nanocrystalline cellulose (NCC)/CdS quantum dots (QDs) nanocomposite was developed for phenol determination. This nanocomposite was prepared with slight modification of nanocrystalline cellulose (NCC) with cationic surfactant of cetyltriammonium bromide (CTAB) and further decorated with 3-mercaptopropionic acid (3-MPA) capped CdS QDs. The nanocomposite material was then employed as scaffold for immobilization of tyrosinase enzyme (Tyr). The electrocatalytic response of Tyr/CTAB-NCC/QDs nanocomposite towards phenol was evaluated using differential pulse voltammetry (DPV). The current response obtained is proportional to the concentration of phenol which attributed to the reduction of *o*-quinone produced at the surface of the modified electrode. Under the optimal conditions, the biosensor exhibits good linearity towards phenol in the concentration range of 5–40 μM (R^2 = 0.9904) with sensitivity and limit of detection (LOD) of 0.078 μA/μM and 0.082 μM, respectively.

1. Introduction

Phenols are one of the toxic pollutant release from various manufacturing industries such as resins and plastic production, wood preservation, petroleum refining, dyes, chemicals, and textiles [1]. According to European Community (EC), the permissible level of phenols in wastewater is around 1 ppm [2]. Nevertheless, due to unsatisfied effluent and water management system, the excess number of phenols has been released into the aquatic environment, exert a harmful effect to human health, concomitantly threatening to biodiversities such as plants, animals, and aquatic life. In particular, phenolic compounds can cause detrimental effects to human health of acute and chronic exposure. Nausea, vomiting, abdominal pain, and diarrhea are common symptoms after exposure to phenol by any route. Prolonged oral or subcutaneous exposure causes damage to the lungs, liver, kidney and genitourinary tract.

Due to its toxicity, several conventional analytical techniques such as spectrophotometry, chromatography, and capillary electrophoresis were employed for phenol quantification. Nevertheless, these techniques are impeded by their technical limitations like tedious, time-consuming, complex to perform, high in cost which limits for on-site and in-situ detection of phenol [3]. In this regards, electrochemical biosensors have been proposed as an excellent alternative technique for phenol determination in the environment with commensurate to other previous conventional methods. Electrochemical biosensors serve as a holistic approach due to their fast response, high selectivity, sensitivity, simplicity, ease of miniaturization and cost effectiveness [4].

Various types of biosensor architecture for the detection of phenol have been reported such as dual-enzyme systems, immunosensors, nucleic acid biosensors, and enzyme biosensors based on oxidative enzymes including tyrosinase (Tyr) [3,5], laccase (Lac) [2,6,7], horseradish peroxidase (HRP) [8,9]. In brief, biosensor involves interaction of analyte (phenol) with a biological species (e.g. enzyme); the biochemical interaction occurs is then translated into a readable electrical signal using a suitable transducer (e.g. electrochemical). Among many enzymes, tyrosinase has received paramount interest due to its ability to undergo electron-transfer reaction without need of additional cofactors in oxidation of phenolic compounds in the presence of oxygen [9,10].

Tyrosinase (Tyr) is also known as monophenol mono-oxygenase is a blue copper protein with coupled binuclear active site [11], which can simultaneously catalyzes two consecutive oxidation reactions: the *o*-hydroxylation of phenols to catechol and subsequently oxidation of catechol to *o*-quinones, hence permitting a wide range of phenolic compounds to be employed as substrates for tyrosinase [11,12]. Apart from its natural substrates (monophenols and *o*-diphenols), Tyr is also capable of oxidizing a variety of aromatic amines and *o*-aminophenols;

* Corresponding author at: Department of Chemistry, Faculty of Science, Universiti Putra Malaysia, 43400 UPM Serdang, Selangor D.E., Malaysia.
E-mail address: jafar@upm.edu.my (J. Abdullah).

https://doi.org/10.1016/j.msec.2019.01.082
Received 5 January 2018; Received in revised form 11 January 2019; Accepted 21 January 2019
Available online 21 January 2019

in which amines are generally hydroxylated to the corresponding *o*-aminophenols, and *o*-aminophenols are oxidized to the corresponding *o*-quinoneimines [14].

In the development of biosensor, selection of suitable solid supports is the pillar factor for providing excellent performance in terms of sensitivity, selectivity, response time, reproducibility and stability [9]. In recent years, various nanomaterials including carbon nanotubes [4,5], graphene [15], conducting polymer [5], Au nanoparticles (AuNPs) [13], nanocrystalline cellulose [16] and quantum dots [17] have been exhaustively employed as immobilization matrices in biosensor architecture with enhanced performance.

To date, NCC has positioned as one of the most promising biocompatible matrices for enabling biomolecules immobilization due to its uniqueness such as large surface area, high aspect ratio, high and specific stiffness and strength, and lack of apparent toxicity [18]. Consequently, the diffusion of analyte become faster, resulting in higher sensitivity and short response time. However, NCC has several shortcomings such as insulating material and too hydrophilic which cause it not conductive and easily dissolved in aqueous solution. In order to enhance the conductivity of NCC, numerous innovative transformation of NCC from an intrinsically insulating material into highly conductive materials has been explored. To diversify NCC in the biosensor application, slight surface modification of NCC with cationic surfactant like cetyltriammonium bromide (CTAB) [19] is necessary to render its moderate hydrophobicity [11].

Colloidal semiconductor quantum dots (QDs) are nanomaterials that widely used in both optical and electrochemical biosensor due to their unique properties such as interesting excitation wavelength-dependent optical emission, high surface area, versatility in surface modification and slightly conductive [20]. However, QDs alone is quite unstable on the bare surface of electrode thus it requires suitable support to deliver its application.

In the present paper, we report a novel electrochemical biosensor based on modified CTAB-NCC/MPA-QDs/Tyr for phenol determination. The hybridization of cetyltriammonium bromide functionalized NCC (CTAB-NCC) with QDs capped 3-mercaptopropionic acid (MPA-QDs) was exploited to improve the performance of the developed biosensor such as sensitivity, selectivity and rapid detection.

This nanocomposite material also offers many advantages as immobilization matrix in term of improve conductivity, biocompatibility, good-film forming capability and high surface area. To the best of our knowledge, there is no previous work reported on the construction of biosensor based on CTAB-NCC/QDs nanocomposites for tyrosinase biosensor.

2. Experimental

2.1. Reagents and solutions

Tyrosinase (EC 1.14.18.1, 50 U mg^{-1}) from mushroom, potassium ferricyanide ($K_3[Fe(CN)_6]$), cetyltrimethylammonium bromide (CTAB), sodium sulfide nonahydrate ($Na_2S{\cdot}9H_2O$), 3-mercaptopropionic acid (3-MPA) and cadmium chloride decahydrate ($CdCl_2{\cdot}10H_2O$) were purchased from Sigma-Aldrich (Germany). Nanocrystalline cellulose (NCC) with 0.94 wt% sulfur on dry NCC sodium form was obtained from University of Maine (USA). Phosphate buffer solution (PBS) was prepared using sodium dihydrogen phosphate anhydrous and di-sodium hydrogen anhydrous salts from HmbG Chemical (Germany).

Methanol (HPLC grade) and acetic acid (AR grade) procured from Merck (Germany) was used for validation using HPLC instrumentation. Other reagents were of analytical grade and used without further purification. All aqueous solutions were prepared using ultrapure water of resistivity (18.2 MΩ-cm) purified using Thermo Scientific water purification system. The dilution of phenolic solutions in 0.1 M phosphate buffer solution (PBS) was freshly prepared daily.

2.2. Apparatus

Screen printed carbon electrode (SPCE) was purchased from Rapid Lab Sdn Bhd (Malaysia) consist of working electrode (carbon), reference electrode (AgCl) and an auxiliary electrode (carbon). Cyclic voltammetry (CV), electrochemical impedance spectroscopy (EIS) and differential pulse voltammetry (DPV) analysis have been conducted using Autolab PGSTAT302N electrochemical workstation (Netherlands).

The surface morphology of the bare and modified SPCE was studied using field emission scanning electron microscopy (FESEM) equipped with energy dispersive X-ray spectroscopy (EDX) on NOVA NANOSEM 230 (FEI Company, USA). The FTIR spectra of the samples were obtained at ambient temperature using the KBr disc method. The disc containing 1 mg of the sample was recorded in the wavenumber range of 500–4000 cm^{-1} using a series 100 Perkin Elmer FTIR 1650 spectrophotometer (USA).

2.3. Preparation of NCC/QDs nanocomposite

The water-soluble CdS QDs was prepared using 3-mercaptopropionic acid as the capping agent according to the previous reported method with slight modification [21]. Typically, 0.5 mmol of $CdCl_2$ and 0.5 mmol of 3-MPA was dissolved in 250 mL of deionized water. The pH 6.0 was adjusted by the addition of 0.1 M of NaOH solution into the solution under constant stirring. The solution was deaerated with N_2 gas for 1 h and then 0.5 mmol of $Na_2S{\cdot}9H_2O$ was injected into the solution under N_2 environment and the solution gradually turned yellowish. Finally, the mixture solution was left overnight with continuous stirring at room temperature.

Surface functionalization of nanocrystalline cellulose (NCC) with cetyltrimethylammonium bromide (CTAB) was conducted with slight modification based on previously reported work [20,25] as follow: NCC suspension (1%, w/v) was prepared by dissolving 0.5 g NCC powder in 50 mL deionized water followed by sonication for 30 min. Then, the pH of NCC suspension was adjusted to 10 using 0.1 M of NaOH solution. The NCC suspension then was added dropwise in the desired amount of CTAB solution, and the foamy mixture was kept at 60 °C for 3 h. The heat was turned off and the reaction was left stirring at room temperature overnight. The suspension was then centrifuged for 10 min at 4000 rpm to remove any possible excess of CTAB that unabsorbed on the NCC. The NCC pelleted was re-dispersed in deionized water and ready to be used.

2.4. Preparation of CTAB-NCC/QDs/Tyrosinase modified SPCE

For the preparation of CTAB-NCC/QDs nanocomposite, CTAB-NCC suspension was added to CdS QDs solution with ratio of 1 to 1 (v/v) and the mixture was vortexed for 5 min until a homogeneous suspension was obtained. Then, 7 µl of CTAB-NCC/QDs mixture was drop casted onto the surface of working electrode of SPCE and kept at room temperature for drying purposes. The prepared CTAB-NCC/QDs modified SPCE was then washed with deionized to remove any unbound nanocomposite and kept in desiccated for further use.

For preparation of biosensor, firstly, 10.0 mg of tyrosinase (Tyr) was dissolved in 1.0 ml of 0.1 M phosphate buffer solution (PBS). Then, 3 µl of Tyr was deposited onto modified CTAB-NCC/QDs and kept at 4 °C for drying process. Finally, CTAB-NCC/QDs/Tyr modified SPCE was thoroughly washed with PBS to remove any unbound Tyr on the surface of SPCE and stored at 4 °C prior to use.

2.5. Electrochemical characterization

The electrochemical characterization of bare SPCE, SPCE modified with NCC, CTAB-NCC and CTAB-NCC/QDs were investigated by using cyclic voltammetry (CV) in the potential window of −0.8 to 0.6 V at the

scan rate of 100 mV/s. The stepwise modification of the electrode has been verified by electrochemical impedance spectroscopy (EIS). Both EIS and CV analysis was performed in 50 mM $[Fe(CN)_6]^{3-}$ containing 0.1 M KCl. Finally, the determination of phenols was carried out using differential pulse voltammetry (DPV) in the potential range of −0.3 to 0.0 V in PBS (pH 7.0) under the following protocol [22]: the response of the biosensor, i.e. the differential voltammetric response of one array from the device was recorded after injecting analyte aliquot. Several analyte aliquots were injected to the electrochemical cell in order to span a wide concentration range. All the analytical performance figures of merit were assessed on the basis of three replicate measurements and error bars are shown in the figures.

2.6. Comparison of the biosensor and HPLC analysis of spiked real sample

The response of the developed biosensor towards various concentration of phenol was compared with high-performance liquid chromatography (HPLC) method. HPLC (Agilent 1200 series) with UV–Vis detector (wavelength = 270 nm) was used for the chromatographic analysis of phenol in lake water sample. Aliquot amount of lake water sample spiked with phenol was filtered using Nylon membrane filter (0.45 μm pore, 13 mm). A 50 μL of injection loop was utilized to deliver 10 μL of filtrated aliquot samples into an Agilent Eclipse reversed phase C_{18} column (150 mm × 4.6 mm, particle size 5 μm). The mixture of 0.1% acetic acid solution and methanol (70:30, v/v) was used as the mobile phase. The separation was performed at room temperature with a flow rate and volume injection of 1.0 mL/min and 10 μL, respectively.

3. Results and discussion

3.1. Characterization of the prepared CTAB-NCC/QDs

Fig. 1 illustrates the absorption and emission spectra of MPA capped CdS QDs was observed in the wavelength range of 300–800 nm. As can be seen, the absorption spectra with shoulder centered at approximately 395 nm (curve a) and fluorescence emission peak at 520 nm (curve b) were observed. The sharp peak exhibit by fluorescence emission spectra indicates the prepared MPA capped CdS QDs are nearly homogeneous and monodisperse [23].

The surface morphologies of NCC, QDs, CTAB-NCC, and CTAB-NCC/QDs nanocomposite were also characterized using TEM and FESEM to reveal size, homogeneity of the composite, the presence of voids, the dispersion level of the nanoparticles within the continuous matrix, the presence of aggregates and the possible orientation of nanoparticles [24]. The TEM images of NCC and CTAB-NCC show agglomerated whiskers-like structure and the NCC was not affected by the modification. The size ranging approximately 4–10 nm in diameter and

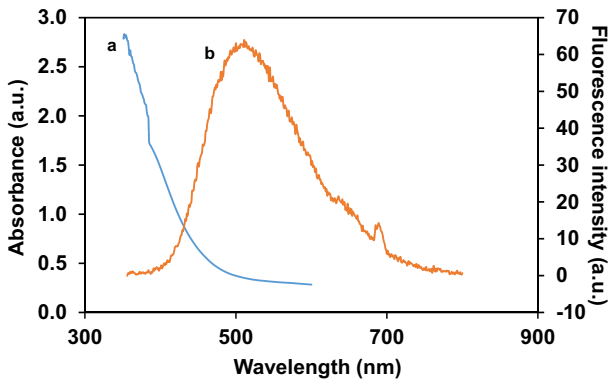

Fig. 1. The spectra of (a) UV–Vis and (b) fluorescence of the synthesized MPA capped CdS QDs.

corresponding length of about 50–100 nm [25] (Fig. 2a, b). For MPA-QDs, the particle is spherical shape, dispersed in size ranging from 2 to 6 nm. This result is in good agreement with previous literature [17,25] (Fig. 2c).

The FESEM reveals the micrographs of CTAB-NCC (Fig. 2d) and CTAB-NCC/QDs (Fig. 2e) nanostructured film analysis at 100 K magnification at room temperature. The CTAB-NCC film exhibited a homogenous, uniform and dense fibrous structures aggregated over the surface of SPCE. This observation is in agreement with previous reported work where well distributed of NCC/polypyrrole on SPE was obtained [16]. For CTAB-NCC/QDs nanocomposite film (Fig. 2e), CdS QDs was appeared like tiny white dots which is similar observation with previous reported work [17].

EDX of selected area was utilized for elemental analysis of CTAB-NCC and CTAB-NCC/QDs nanocomposite film. The EDX patterns with elemental composition illustrated in Fig. 2 (f and g). For CTAB-NCC/QDs nanocomposite films (Fig. 2g), the presence of respective elemental of C, O, S and Cd, indicating the CdS QDs was successfully decorated into the CTAB-NCC films.

FTIR analysis was attempted to characterize the surface modification interaction by comparing the spectra of (a) NCC (b) CTAB-NCC, and (c) CTAB-NCC/QDs (Fig. 3). All spectra have the same backbone only slightly change in the absorption bands was observed. The absorption peaks between 3650 and 3200 cm^{-1} are mainly assignable to intra- and intermolecular O—H and CH_2—OH stretching vibrations [26]. The spectral band at 2900 cm^{-1} can be seen in all samples, and it is more intense in CTAB-NCC (curve b) and CTAB-NCC/QDs (curve c) due to the C—H stretching from the long alkyl chain of CTAB [27]. This demonstrates that CTAB successfully doped onto the NCC. The new formation of a peak at 1480 cm^{-1} was observed in CTAB-NCC (curve b). Based on previous literature, the peak is due to the C—H bending of cationic substituent of CTAB [28]. The C—O stretching and C═O was located at 1030 cm^{-1} and 1647 cm^{-1}, respectively. The band becomes smaller and slightly shifted in both CTAB-NCC and CTAB-NCC/QDs. This observation suggests that there is an electrostatic interaction between the NCC with CTAB and QDs because they possess opposite charges [29].

The surface charge of the nanoparticles was also assessed using the Malvern Zetasizer. The unmodified NCC with surface charge potential value of −40.55 ± 5.06 mV was observed. This is because the NCC was obtained via acid hydrolysis using sulfuric acid. The NCC functionalized CTAB shows surface charge potential of +33.27 ± 1.50 mV.

Meanwhile, the surface charge value of MPA-QDs is −35.63 ± 4.01 mV. This magnitude of potential indicates that both nanoparticles have stable suspension as both of the values lie outside −30 mV to +30.50 mV range represents good suspension stability.

Remarkably, both CTAB-NCC and MPA-QDs carried opposite surface charge, thus, when CTAB-NCC decorated with MPA-QDs electrostatic interaction between a positively charged of CTAB-NCC and negatively charged of MPA-QDs is occurred. It is expected that the interaction between opposite charge materials form strong electrostatic force and attached to each other produced the formation of CTAB-NCC/QDs nanocomposite. This nanocomposite serves as a stable platform for enzyme immobilization without the loss of protein structure or activity, which corresponds to previous work using negatively charged surface of TiO_2 and positively charged surface of lysine and/or arginine [30].

3.2. Electrochemical characterization of CTAB-NCC/QDs modified SPCE

Cyclic voltammetry (CV) was utilized to investigate the interface kinetics on the surface of bare SPCE and SPCE modified with NCC, CTAB-NCC, CTAB-NCC/QDs using potassium ferrocyanide solution to observe amount of charge passed during CV cycle [31]. Fig. 4 illustrated the voltammogram of bare SPCE (curve a) (the value of I_{pa} = 104.58 μA and I_{pc} = −141.14 μA) and NCC (curve b) (with anodic peak current I_{pa} = 106.80 μA and cathodic peak current

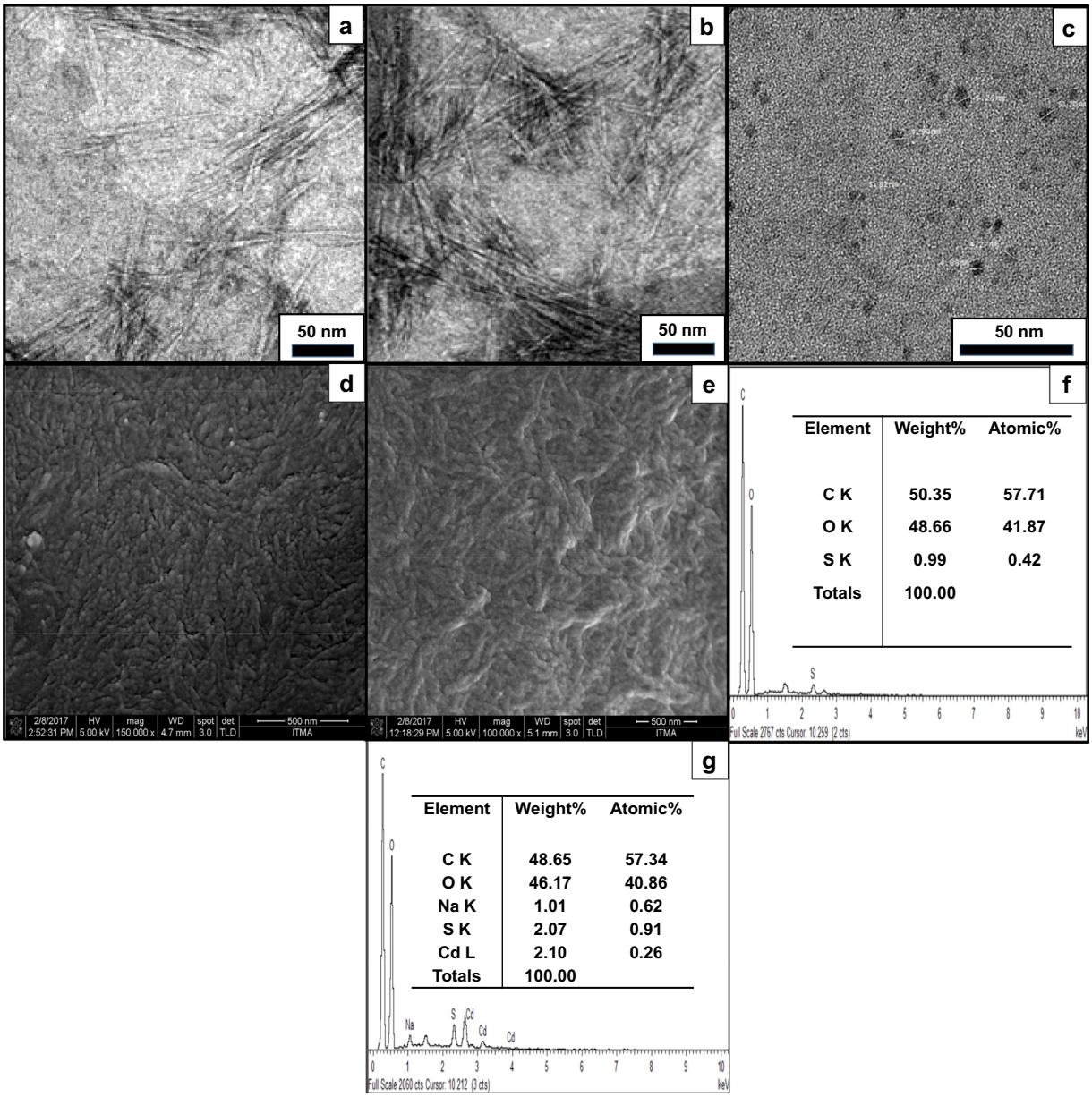

Fig. 2. The TEM images for (a) NCC, (b) CTAB-NCC, and (c) MPA-QDs, the FESEM micrograph of (d) CTAB-NCC nanostructured film, (e) CTAB-NCC/QDs nanocomposite film, and EDX analysis of (f) CTAB-NCC nanostructured film, (g) CTAB-NCC/QDs nanocomposite film.

$I_{pc} = -146.94\,\mu A$) have no significant change in the peak currents. The NCC is hydrophilic in nature [32] due to the presence of hydroxyl group on its surface. This behavior makes it easily dissolve in aqueous solution and could probably detach from the surface of electrode.

Hence, NCC requires surface modification in order to alter its hydrophilicity to form slightly hydrophobic, concomitantly serves as a promising matrix for attaching metallic nanoparticles for further applications [33]. Surface modification of NCC by using surfactant offers facile and promising technique to alter the surface chemistry and tailor colloidal stability in many applications. Modification of NCC employing CTAB has been studied previously; the prepared CTAB-NCC capable of coupled hydrophobic anti-cancer drugs into the matrix and delivered a controlled drug release [19]. In other study, it was also discovered the use of CTAB-NCC to facilitate metal nanoparticle into the matrix [32].

In Fig. 4, CTAB-NCC (curve c) (the value of $I_{pa} = 113.95\,\mu A$ and $I_{pc} = -204.10\,\mu A$) and CTAB-NCC/QDs modified SPCE (curve d) (the value of $I_{pa} = 165.90\,\mu A$ and $I_{pc} = -248.66\,\mu A$, shows higher peak current response compared to bare SPCE (curve a). It is clearly illustrated that higher current response is associated with higher surface area and good conductivity of the CTAB-NCC/QDs modified SPCE. The peak-to-peak separation, ΔE_p for bare, NCC, CTAB-NCC, and CTAB-NCC/QDs modified SPCE were gradually decreased following the order from 54.90 mV to 40.70 mV demonstrated a fast and reversible electron transfer process [17].

Electrochemical impedance spectroscopy (EIS) is a simple and sensitive analysis to study the change of electrode interface and complex electrical resistance of a system. The electrochemical impedance spectroscopic data of Tyr/CTAB-NCC/QDs was fitted using simple equal circuit, which shown in Fig. 5 (inset), which comparable to another report [34]. In this circuit, R_s, Z_w, CPE, and R_{ct} represent solution resistance; Warburg impedance, constant phase element, and charge transfer resistance, respectively.

Fig. 5 shows Nyquist plot of the different modified SPCE composed of a semicircle portion and linear portion. The semicircular curve at higher frequencies demonstrates the charge-transfer-limited process; meanwhile the linear line demonstrates the diffusion-limited process.

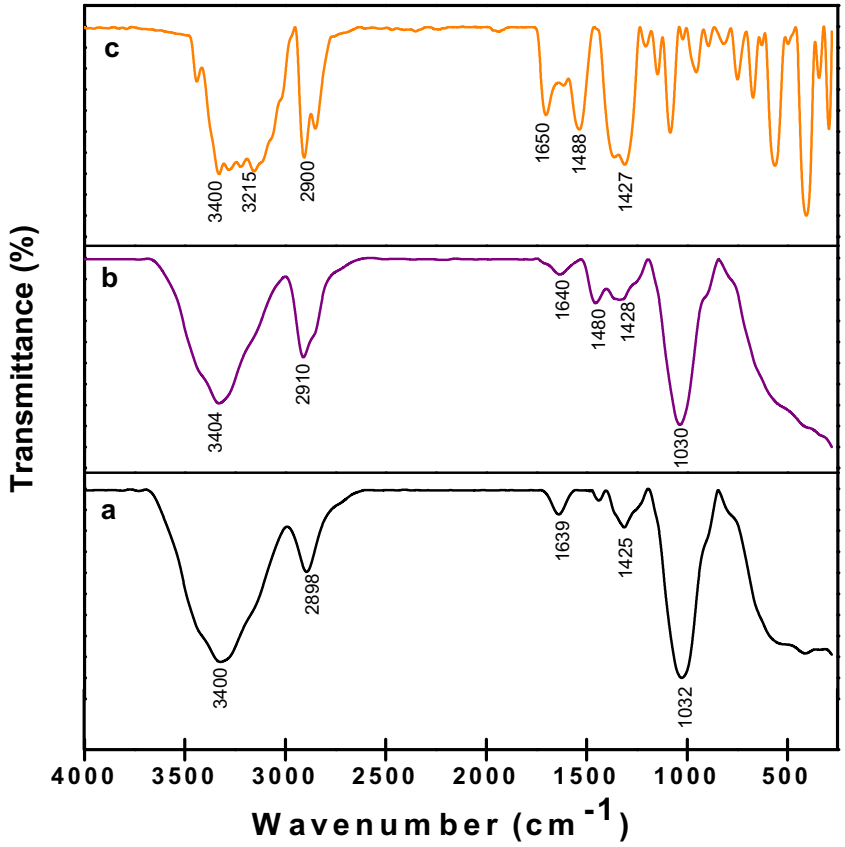

Fig. 3. The FTIR spectra for (a) NCC only, (b) CTAB-NCC, and (c) CTAB-NCC/QDs nanostructured film.

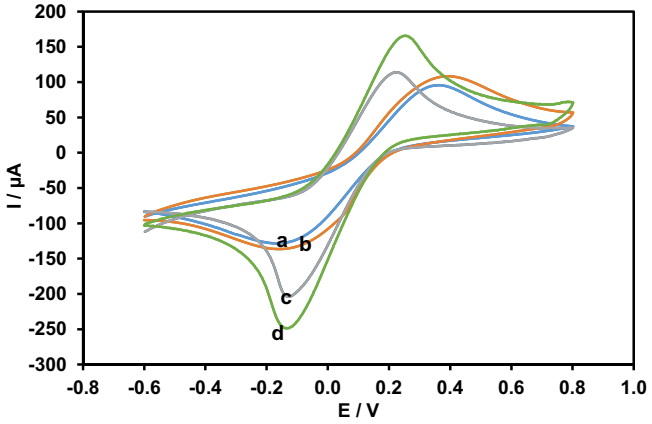

Fig. 4. CVs for (a) bare, (b) NCC, (c) CTAB-NCC and (d) CTAB-NCC/QDs modified SPCE in 5 mM $K_3Fe(CN)_6$/0.1 M KCl with scan rate of 100 mV/s.

Basically, the semicircle diameter corresponds to the charge-transfer resistance (R_{ct}) [35]. The bare SPCE and NCC modified SPCE shows a larger - diameter semicircle with the R_{ct} value of 20,200 Ω and 20,300 Ω, respectively. It is observed that there were no significant changes that can be found in the value of R_{ct} of bare and NCC modified SPCE. It could probably due to the NCC detached from the SPCE surface as cellulose is very hydrophilic easily dissolved in the aqueous solution. Thus, surface modification of NCC is required for the biosensor applications [16].

After the surface modification of the NCC with cationic surfactant (CTAB-NCC), the R_{ct} (181 Ω) is obviously decreased due to improvement of conductivity properties of the modified SPCE [31]. Thus, the CTAB-NCC modified SPCE allowed greater permeation for the $[Fe(CN)_6]^{3-}$ redox probe. Subsequently, the CTAB-NCC/QDs modified SPCE shows slightly lower R_{ct} value of 173 Ω. This may be ascribed to the fact that the CTAB-NCC/QDs nanocomposite films are conductive, and verified that QDs could facilitate the electron transfer [36].

For CTAB-NCC/QDs/Tyr, the R_{ct} was slightly increased with the value of 244 Ω. The increase in resistance of CTAB-NCC/QDs/Tyr modified SPCE indicates that the interface is blocked by Tyr which forming an electron transfer barrier. This observation confirming the successful immobilization of Tyr onto the surface of modified SPCE [37]. Therefore, the improved properties are observed in both of CTAB-NCC and CTAB-NCC/QDs modified SPCE.

3.3. Reaction mechanism of the biosensor

Voltammetric behavior of phenols was further studied using differential pulse voltammetry (DPV) within potential range of −0.3 V to 0.0 V. Fig. 6a displays the typical differential pulse voltammogram (DPV) of phenol in phosphate buffer solution towards SPCE modified with Tyr/NCC, Tyr/CTAB-NCC and Tyr/CTAB-NCC/QDs, respectively. Upon addition of a successive aliquot of phenol into the phosphate buffer solution, slight reduction peak current was obtained with SPCE modified Tyr/NCC and moderate response with SPCE modified Tyr/CTAB-NCC.

As can be seen Fig. 6b, SPCE modified with Tyr/CTAB-NCC/QDs exhibited higher current response compared to Tyr/NCC and Tyr/CTAB-NCC, which indicated that the CTAB-NCC/QDs nanocomposite plays a significant role in the improvement of enzyme immobilization and facilitates the direct electron transfer between the substrate molecules and the modified electrode surface.

Tyrosinase (polyphenol oxidase) is a blue copper protein with 2 copper atoms in the active center), catalyzed the oxidation and hydroxylation of polyphenols. In the present work, tyrosinase (Tyr) has

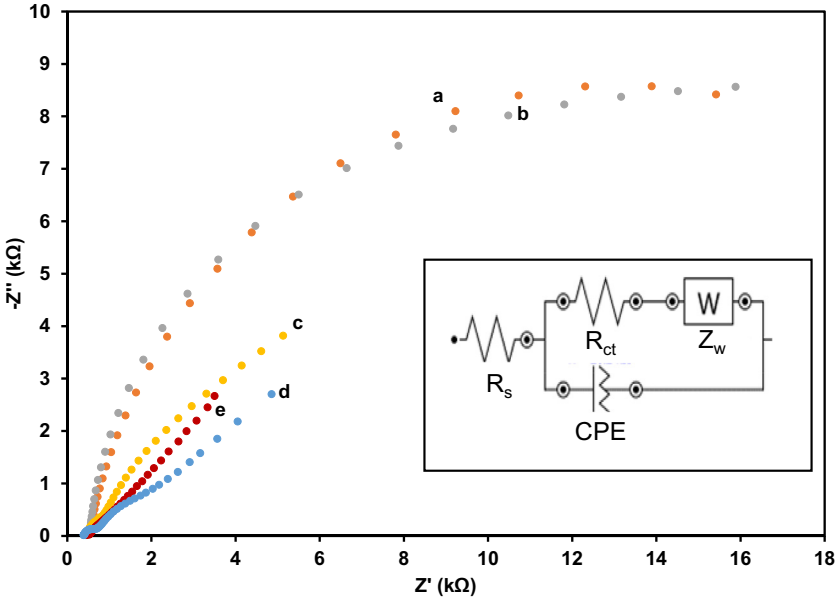

Fig. 5. Nyquist plots of EIS for (a) bare SPCE (b) NCC, (c) CTAB-NCC, and (d) CTAB-NCC/QDs, (e) Tyr/CTAB-NCC/QDs modified SPCE. Inset: Randles equivalent circuit applied to fit the spectroscopic data.

been used as a typical model for the detection of phenols based on Tyr/CTAB-NCC/QDs biosensor. The enzymatic reaction of electrochemical Tyr-biosensor is shown in Schematic 1.

In the presence of oxygen molecule, Tyr catalyzes the oxidation of phenol to the corresponding *o*-quinones through its active center and the oxygen is then reduced to water. Subsequently, the *o*-quinone generated by the previous enzymatic reaction was further reduced to catechol at the surface of the electrode, giving rise to an electrocatalytic

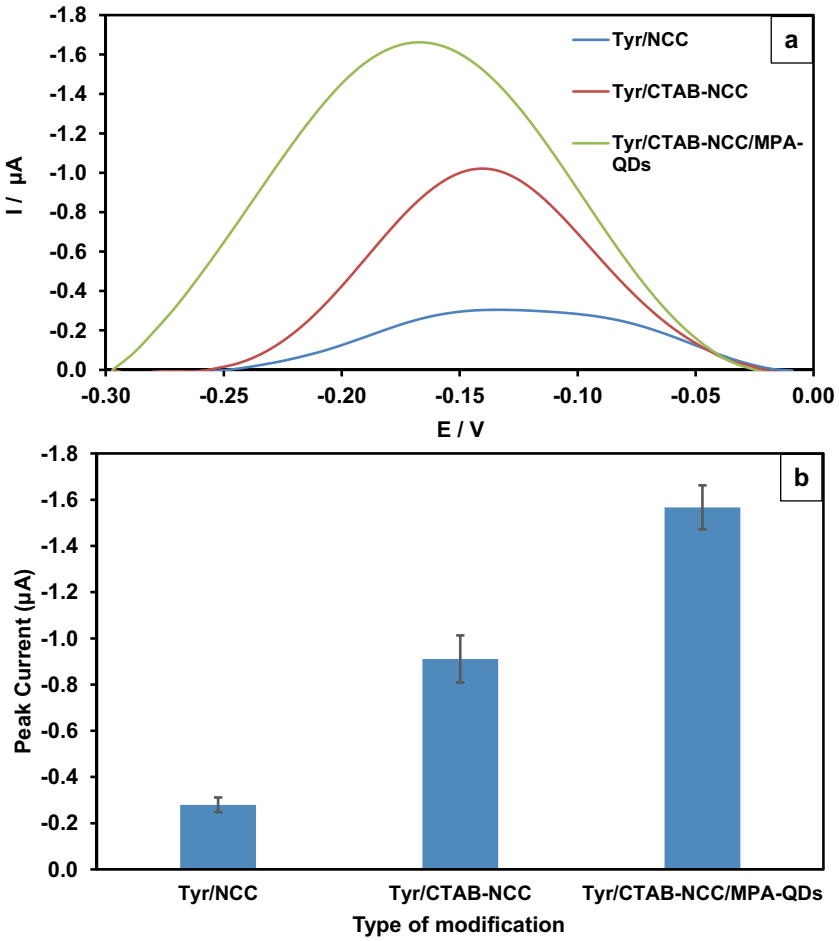

Fig. 6. Plot of (a) DPVs voltammograms, (b) response of different modified electrode of Tyr/NCC, Tyr/CTAB-NCC, Tyr/CTAB-NCC/MPA-QDs towards 10 µM phenol.

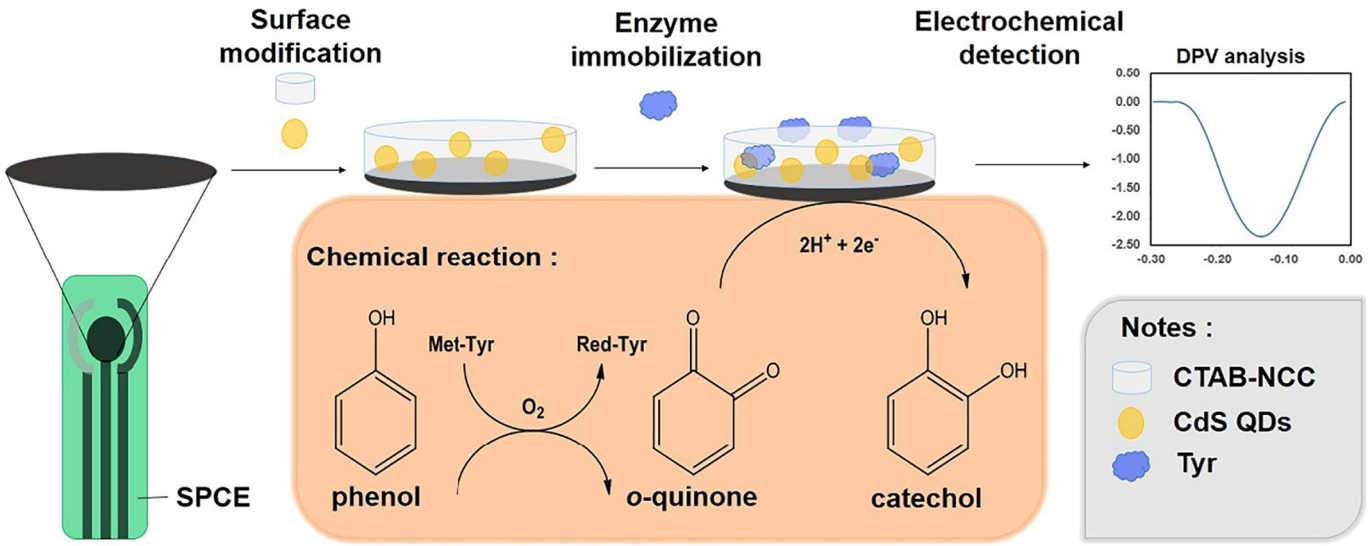

Schematic 1. Schematic representation on the construction of CTAB-NCC/QDs/Tyr/SPCE biosensor.

current response [38]. Based on the mechanism, electrochemical tyrosinase biosensor can be utilized as a feasible device for the detection of phenol.

3.4. Optimization of experimental parameters

In this study, several electroanalytical parameters were thoroughly investigated such as pH, accumulation potential and time, the amount of enzyme, respectively. Influence of pH is one of the significant parameters which related to enzymatic activity and stability of the biosensor in aqueous solution.

The dependency of cathodic peak current (I_{pc}) was investigated in phosphate buffer solution over different pH ranging from 6.0 to 9.0 (Fig. S1). At low pH range, cathodic peak current gradually increase proportionally to increase of enzymatic activity [39]. At higher pH beyond 7.0, the cathodic peak current decrease most probably due to loss or inactivation of the enzyme activity [6]. It was found that the maximum peak achieved at pH 7.0. This result agrees with the optimum pH range of 5.0 to 8.0 reported for free tyrosinase and indicate that the immobilization procedure did not alter the tyrosinase activity. Thus, phosphate buffer solution (PBS) pH 7.0 was used for subsequent experiments.

Accumulation potential plays important role in the biosensor response, where it contributes to the improvement of sensitivity and selectivity of the biosensor. The influence of accumulation potential on the voltammetric response of the biosensor towards phenol was investigated in the potential range of +0.05 to −0.20 V in PBS (pH 7.0) and accumulation time was fixed at 60 s. The most intense response was obtained at −0.2 V. Above potential of −0.20 V, the sensor response starts to decrease. This phenomenon may be due to increase in oxygen depletion in the vicinity of the Tyr immobilized on the surface of SPCE, thus reduce the enzymatic rate which is consistent with previous study [3]. Thus, −0.2 V was implied as optimum accumulation potential for analytical procedures.

The effect of accumulation time on the voltammetric response of the biosensor was also studied in the time frame of 30 s to 180 s. The results illustrated that the cathodic peak current increased within increasing accumulation time up to 60 s, before reaching the adsorption equilibrium [40]. Beyond 60 s, the adsorbed phenol is saturated at the surface of CTAB-NCC/QDs/Tyr modified SPCE. Hence, the time of 60 s is chosen as the optimum accumulation time.

The amount of enzyme immobilized onto the electrode surface is crucial to improve the sensitivity of the biosensor. In particular, the electrochemical response of the electrode as a function of amount of immobilized enzyme was investigated between 2.0 and 20.0 mg/ml. As represented in Fig. S2, the current response increases with the increase of Tyr amount, reaching maximum values of 10 mg/ml of immobilized tyrosinase. Beyond the amount of Tyr of 10 mg/ml, significant decrease in cathodic peak current which could be attributed to film thickness, simultaneously increase the interfacial electron transfer resistance, and decelerate the electron transfer rate [6]. Therefore, 10 mg/ml of tyrosinase was employed for the biosensor development.

3.5. Analytical performance of the developed biosensor

The performance of the developed sensor towards different concentration of analytes under optimum condition was investigated. In this study, the developed sensor shows a well-defined cathodic peak in the dynamic range from 5 to 40 µM (Fig. 7). A linear calibration curve for phenol was obtained with linear regression equations of I_{pa} (A) = 0.078x − 1.7104 (R^2 = 0.9904). Limit of detection (LOD) was calculated according to $3S_b/b$, where S_b is the standard deviation of the blank measurements (n = 3), b is the slope of the calibration curve [2] and the calculated LOD was found to be at 0.082 µM.

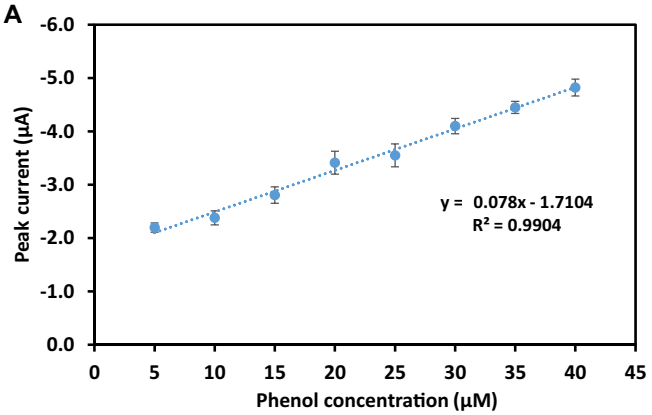

Fig. 7. Calibration curve of the developed sensor towards different concentrations of phenol.
Experimental conditions: 10 µM phenol in 0.1 M of PBS (pH 7.0). Accumulation potential ranging from −0.20 V, accumulation time = 60 s, Tyr conc. = 10 mg/ml. The error bars indicate the standard error (s) for triplicate measurements (n = 3) with same biosensor.

Table 1
Response characteristics of CTAB-NCC/QDs/Tyr modified SPCE to various phenolic compounds.

Phenolic compounds	Linear range (μM)	Detection limit (μM)	Sensitivity (μA/μM)	Correlation coefficient	K_m (μM)
Phenol	5.0–40.0	0.082	0.078	0.994	3.26
Catechol	1.0–25.0	0.125	0.017	0.995	1.23
o-Cresol	2.0–10.0	0.007	0.273	0.986	11.14
4-Chlorophenol	5.0–25.0	0.021	0.102	0.928	11.47

Table 2
The influence of potential interferents on DPVs response of phenol detection.

	Interference	Concentration (μM)	Signal change (μA)	Relative error (%)
Organic	Glucose	10	0.011	3.06
	Ascorbic acid	10	0.017	4.86
	Uric acid	10	0.015	4.30
	Caffeine	10	0.013	3.70
Inorganic	Cu^{2+}	100	0.013	2.31
	Fe^{2+}	100	0.004	1.48
	Zn^{2+}	100	0.011	3.73
	Mg^{2+}	100	0.003	3.38

The performance of the enzyme electrode towards other phenols such as catechol, m-cresol and 4-chlorophenol were also investigated using DPV under optimum experimental condition. The detection characteristic of the biosensor for different phenols, including linearity range, correlation coefficient, sensitivity, and detection limits was tabulated in Table 1. The enzymatic biosensor gave the linearity range of 5.0–40.0 μM (0.47–3.76 mg/L) (R^2 = 0.994), 1.0 to 25.0 μM (0.11–2.75 mg/L) (R^2 = 0.995), 2.0 to 10.0 μM (0.22–1.08 mg/L) (R^2 = 0.986), 5.0 to 25.0 μM (0.64–3.21 mg/L) (R^2 = 0.928), and LOD of 0.082 μM (0.0077 mg/L), 0.125 μM (0.0138 mg/L), 0.007 μM (0.0008 mg/L), 0.021 μM (0.0026 mg/L) for phenol, catechol, *o*-cresol and 4-chlorophenol, respectively. Moreover, the sensitivity of SPCE/CTAB-NCC/QDs/Tyr following the order of *o*-cresol > 4-chlorophenol > phenol > catechol. The response characteristic observed from different types of phenols most prominently depends on the Tyr catalytic selectivity for different compounds [11].

The kinetic behavior of the enzyme electrode was also studied in this work. The apparent Michaelis-Menten constant, K_m indicates the enzyme-substrate kinetics for the enzyme electrode; the smaller the K_m value, the greater the affinity for the substrate. By using Lineweaver-Burk plot, the K_m values obtained were 3.26, 1.23, 11.14 and 11.47 for phenol, catechol, *o*-cresol, and 4-chlorophenol, respectively. The result shows that the CTAB-NCC/QDs lead to the high affinity of the enzyme following the order of catechol, phenol, *o*-cresol and 4-chlorophenol. The low K_m values resulting high entrapped Tyr onto the matrix of CTAB-NCC/QDs nanocomposites, thus provide high affinity to phenols [3].

Reproducibility study of CTAB-NCC/QDs/Tyr modified SPCE were evaluated at phenol concentration of 10 μM in phosphate buffer solution (pH 7.0) and the relative standard deviation (RSD) of 2.69% (n = 5) was obtained. The repeatability of the developed biosensor was also examined and the RSD was found to be 6.75% (n = 5), signifying the fouling of the surface of SPCE due to the formation of non-conducting oxidation products of phenol or change in the morphology of the surface of SPCE [8].

The long-term stability of the biosensor stored at 4 °C was evaluated periodically within 5 weeks. The response of CTAB-NCC/QDs/Tyr modified SPCE was remains unchanged during the first two weeks of storage and retained approximately 75% of its original response after 5 weeks of storage. As a nanomaterial, cytotoxicity of CdS QDs may influence the stability of the biological material (enzyme) used in this study and effect to the environment. In this work, low amount of CdS QDs used in the immobilization matrix would probably reduce the cytotoxicity of the QDs. Li et al. [41] had reported the CdS QDs with MPS-replaced plus silica capping showed less cytotoxicity than those with MPA-capping and MPS-replaced capping. Thus, it is also expected MPA capped CdS QDs functionalized with CTAB-NCC exhibited less cytotoxicity compared to CdS QDs.

3.6. Interference study and real sample analysis of CTAB-NCC/QDs/Tyr modified SPCE

The influence of any possible interfering substances on the proposed biosensor was investigated in order to evaluate the selectivity of the biosensor towards the substrate. Several organic interference with ten times concentrations, including glucose, ascorbic acid, uric acid, and caffeine, while inorganic substances of heavy metal ions with hundred times concentration, such as Fe^{2+}, Cu^{2+}, Zn^{2+}, and Mg^{2+} were added separately into 1 μM of phenol solution. As can be seen in Table 2, the organic and inorganic interference produced less than ± 5% relative error on the phenol detection. This result indicates that the proposed CTAB-NCC/QDs/Tyr modified SPCE exhibit no significant interference in the presence of the above species, indicating good selectivity to phenol.

3.7. Comparison of the biosensor and HPLC analysis of spiked real sample

In addition, to evaluate the potential application of the proposed biosensor in real samples analysis, the performance of the biosensor for the analysis of water sample spiked with phenol was tested and compared with the HPLC method. The water sample was collected from the lake near Universiti Putra Malaysia, UPM Serdang, Selangor and was used for quantitative analysis. For unspiked water sample, no phenol was observed by the developed method and HPLC technique; verified that the sample was absent with phenol. Therefore, the standard addition method was applied to investigate the performance of the proposed biosensor.

The lake water sample was spiked with six different known concentrations of phenol in the range of 5 μM to 30 μM. The results from the water samples recovery are summarized in Table 3. The results were compared with those measured using HPLC method. The results demonstrate that the biosensor and HPLC method recovered about 97–104% and 88–91% of the phenol in the water samples, respectively.

Statistical analysis for comparing the two means of the developed biosensor and HPLC method was also evaluated. Overall the calculated *t*-test value of the samples are less than the critical value (t_4 = 2.78) which confirm that the developed biosensor and HPLC method display a good agreement and comparable.

4. Conclusions

In summary, phenol biosensor based on tyrosinase immobilized on CTAB-NCC/MPA-QDs modified SPCE was successfully designed. The CTAB-NCC/QDs nanocomposite offered special characteristics of two components which provide improved conductivity, good biocompatibility, and permeability microenvironment with high affinity entrapment towards enzyme immobilization. The proposed biosensor demonstrates good analytical performances with wide detection range of 5–40 μM (0.47–3.76 mg/L), sensitivity of 0.078 μA/μM and detection

Table 3
A comparison between the developed tyrosinase biosensor and HPLC method.

Water sample	Added (μM)	The developed method (μM) (n = 3)	Recovery (%)	HPLC method (μM) (n = 3)	Recovery (%)	*t*-Test
Lake water	5.0	4.951 ± 0.167	99.03	4.356 ± 0.002	87.12	0.31
	10.0	10.445 ± 0.664	104.35	8.893 ± 0.005	88.93	2.02
	15.0	15.447 ± 1.395	102.90	13.271 ± 0.014	87.58	1.35
	20.0	20.762 ± 1.624	103.79	18.137 ± 0.014	90.69	1.40
	25.0	25.606 + 1.042	102.39	22.399 ± 0.006	89.60	2.67
	30.0	29.157 ± 1.077	97.15	26.435 ± 0.006	88.12	2.19

Note: The critical value, $t_4 = 2.78$ ($p = 0.05$).

limit of 0.082 μM (0.0077 mg/L), respectively. The biosensor remained its activity and stability for at least one month, shows good electrochemical activity with high sensitivity and selectivity. A comparison study on analysis of spiked real sample by using the developed sensor and HPLC method have shown good agreement and comparable. The designed electrochemical biosensor exhibits excellent features and could be potentially applied for the determination of phenols in the environmental samples.

Acknowledgments

The authors are gratefully acknowledged the financial support provided by the Malaysian Government through its Ministry of Science, Technology and Innovation, Malaysia under Science Fund (03-01-04-SF2045) and Ministry of Education under Fundamental Research Grant Scheme (FRGS/1/2012/SG01/UPM/02/1).

Appendix A. Supplementary data

Supplementary data to this article can be found online at https://doi.org/10.1016/j.msec.2019.01.082.

References

[1] H. Guan, X. Liu, W. Wang, Encapsulation of tyrosinase within liposome bioreactors for developing an amperometric phenolic compounds biosensor, J. Solid State Electrochem. 17 (2013) 2887–2893.
[2] M. Nazari, S. Kashanian, R. Rafipour, Laccase immobilization on the electrode surface to design a biosensor for the detection of phenolic compound such as catechol, Spectrochim. Acta A 145 (2015) 130–138.
[3] E. Han, Y. Yang, Z. He, J. Cai, X. Zhang, X. Dong, Development of tyrosinase biosensor based on quantum dots/chitosan nanocomposite for detection of phenolic compounds, Anal. Biochem. 486 (2015) 102–106.
[4] J. Kochana, K. Wapiennik, J. Kozak, P. Knihnicki, A. Pollap, M. Wo, J. Nowak, P. Ko, Tyrosinase-based biosensor for determination of bisphenol A in a fl ow-batch system, Talanta 144 (2015) 163–170.
[5] C. Lete, S. Lupu, B. Lakard, J. Hihn, F. Javier, Multi-analyte determination of dopamine and catechol at single-walled carbon nanotubes – conducting polymer – tyrosinase based electrochemical biosensors, J. Electroanal. Chem. 744 (2015) 53–61.
[6] M. Portaccio, D. Di Tuoro, F. Arduini, D. Moscone, M. Cammarota, Laccase biosensor based on screen-printed electrode modified with thionine – carbon black nanocomposite, for Bisphenol A detection, Electrochim. Acta 109 (2013) 340–347.
[7] X. Liu, L. Luo, Y. Xu, Amperometric biosensors based on alumina nanoparticles-chitosan-horseradish peroxidase nanobiocomposites for the determination of phenolic compounds, Analyst 4 (2011) 696–701.
[8] N. Negash, H. Alemu, M. Tessema, Electrochemical characterization and determination of phenol and chlorophenols by voltammetry at single wall carbon nanotube/poly(3, 4-ethylenedioxythiophene) modified screen printed carbon electrode, Int. Sch. Res. Not. 2015 (2015) 1–11.
[9] K. Lasmi, H. Derder, A. Kermad, S. Sam, H. Boukhalfa-Abib, S. Belhousse, F.Z. Tighilt, K. Hamdani, N. Gabouze, Tyrosinase immobilization on functionalized porous silicon surface for optical monitoring of pyrocatechol, Appl. Surf. Sci. 446 (2018) 3–9.
[10] J. Abdullah, M. Ahmad, N. Karuppiah, L.Y. Heng, H. Sidek, Immobilization of tyrosinase in chitosan film for an optical detection of phenol, Sensors Actuators B 114 (2006) 604–609.
[11] S. Hashemnia, S. Khayatzadeh, M. Hashemnia, Electrochemical detection of phenolic compounds using composite film of multiwall carbon nanotube/surfactant/tyrosinase on a carbon paste electrode, J. Solid State Electrochem. 16 (2012) 473–479.
[12] F. Campanhã, B.C. Janegitz, C.M.A. Brett, O. Fatibello-filho, Chemical tyrosinase biosensor based on a glassy carbon electrode modified with multi-walled carbon nanotubes and 1-butyl-3-methylimidazolium, Sensors Actuators B 188 (2013) 10–13.
[13] N. Karim, H. Jin, Amperometric phenol biosensor based on covalent immobilization of tyrosinase on Au nanoparticle modified screen printed carbon electrodes, Talanta 116 (2013) 991–996.
[14] L. Del Torno-De Román, M. Asunción Alonso-Lomillo, O. Domínguez-Renedo, M. Julia Arcos-Martínez, Tyrosinase based biosensor for the electrochemical determination of sulfamethoxazole, Sensors Actuators B 227 (2016) 48–53.
[15] Y. Zhao, D. Huo, J. Bao, M. Yang, M. Chen, J. Hou, H. Fa, C. Hou, Biosensor based on 3D graphene-supported Fe_3O_4 quantum dots as biomimetic enzyme for in situ detection of H_2O_2 released from living cells, Sensors Actuators B 244 (2017) 1037–1044.
[16] C. Esmaeili, M.M. Abdi, A.P. Mathew, M. Jonoobi, K. Oksman, M. Rezayi, Synergy effect of nanocrystalline cellulose for the biosensing detection of glucose, Sensors 15 (2015) 24681–24697.
[17] M. Hazani, M. Zaid, J. Abdullah, N. Azah, Y. Sulaiman, PNA biosensor based on reduced graphene oxide/water soluble quantum dots for the detection of Mycobacterium tuberculosis, Sensors Actuators B 241 (2017) 1024–1034.
[18] V. Incani, C. Danumah, Y. Boluk, Nanocomposites of nanocrystalline cellulose for enzyme immobilization, Cellulose 20 (2013) 191–200.
[19] T. Abitbol, H. Marway, E.D. Cranston, Surface modification of cellulose nanocrystals with cetyltrimethylammonium bromide, Nord. Pulp Pap. Res. J. 29 (2014) 46–57.
[20] V.A. Online, H. Huang, J. Zhu, The electrochemical applications of quantum dots, Analyst 20 (2013) 5855–5865.
[21] T. Madrakian, S. Maleki, M. Heidari, A. Afkhami, An electrochemical sensor for rizatriptan benzoate determination using Fe_3O_4 nanoparticle/multiwall carbon nanotube-modified glassy carbon electrode in real samples, Mater. Sci. Eng. C 63 (2016) 637–643.
[22] C. Lete, B. Lakard, J. Hihn, F. Javier, S. Lupu, Use of sinusoidal voltages with fixed frequency in the preparation of tyrosinase based electrochemical biosensors for dopamine electroanalysis, Sensors Actuators B 240 (2017) 801–809.
[23] N.E. Azmi, N.I. Ramli, J. Abdullah, M.A. Abdul Hamid, H. Sidek, S. Abd Rahman, N. Ariffin, N.A. Yusof, A simple and sensitive fluorescence based biosensor for the determination of uric acid using H_2O_2-sensitive quantum dots/dual enzymes, Biosens. Bioelectron. 67 (2015) 129–133.
[24] A. Khan, R.A. Khan, S. Salmieri, C. Le Tien, B. Riedl, J. Bouchard, G. Chauve, V. Tan, M.R. Kamal, M. Lacroix, Mechanical and barrier properties of nanocrystalline cellulose reinforced chitosan based nanocomposite films, Carbohydr. Polym. 90 (2012) 1601–1608.
[25] N. Zainuddin, I. Ahmad, H. Kargarzadeh, S. Ramli, Hydrophobic kenaf nanocrystalline cellulose for the binding of curcumin, Carbohydr. Polym. 163 (2017) 261–269.
[26] T. Madrakian, S. Maleki, A. Afkhami, Surface decoration of cadmium-sulfide quantum dots with 3-mercaptopropionic acid as a fluorescence probe for determination of ciprofloxacin in real samples, Sensors Actuators B 243 (2017) 14–21.
[27] K. Singh, J. Kumar, A.T. Jai, M. Sinha, Functionalization of nanocrystalline cellulose for decontamination of Cr(III) and Cr(VI) from aqueous system: computational modeling approach, Clean Techn. Environ. Policy 16 (2014) 1179–1191.
[28] M. Zaman, H. Xiao, F. Chibante, Y. Ni, Synthesis and characterization of cationically modified nanocrystalline cellulose, Carbohydr. Polym. 89 (2012) 163–170.
[29] H.T. Lian, B. Liu, Y.P. Chen, X.Y. Sun, A urea electrochemical sensor based on molecularly imprinted chitosan film doping with CdS quantum dots, Anal. Biochem. 426 (2012) 40–46.
[30] W. Zhao, J. Xu, H. Chen, Photoelectrochemical enzymatic biosensors, Biosens. Bioelectron. 92 (2017) 294–304.
[31] J. Fan, W. Shao, G. Xu, T. Cui, X. Luo, Preparation and electrochemical catalytic application of nanocrystalline cellulose doped, RSC Adv. 46 (2014) 24328–24333.
[32] L. Jasmani, S. Adnan, Preparation and characterization of nanocrystalline cellulose from Acacia mangium and its reinforcement potential, Carbohydr. Polym. 161 (2017) 166–171.
[33] E. Lam, K.B. Male, J.H. Chong, A.C.W. Leung, J.H.T. Luong, Applications of functionalized and nanoparticle-modified nanocrystalline cellulose, Trends Biotechnol. 30 (2012) 283–290.
[34] L. Mei, J. Feng, L. Wu, J. Zhou, J. Chen, A. Wang, Novel phenol biosensor based on laccase immobilized on reduced graphene oxide supported palladium–copper alloyed nanocages, Biosens. Bioelectron. 74 (2015) 347–352.
[35] J. Zhang, T. Kang, Y. Hao, L. Lu, S. Cheng, Electrochemiluminescent immunosensor based on CdS quantum dots for ultrasensitive detection of microcystin-LR, Sensors Actuators B 214 (2015) 117–123.
[36] X. Tan, Q. Hu, J. Wu, X. Li, P. Li, H. Yu, X. Li, F. Lei, Electrochemical sensor based

on molecularly imprinted polymer reduced graphene oxide and gold nanoparticles modified electrode for detection of carbofuran, Sensors Actuators B 220 (2015) 216–221.
[37] J. Li, T. Gao, S. Gu, J. Zhi, J. Yang, G. Li, An electrochemical biosensor for the assay of alpha-fetoprotein-L3 with practical applications, Biosens. Bioelectron. 87 (2017) 352–357.
[38] X. Liu, R. Yan, J. Zhu, J. Zhang, X. Liu, Growing TiO_2 nanotubes on graphene nanoplatelets and applying the nanonanocomposite as scaffold of electrochemical tyrosinase biosensor, Sensors Actuators B 209 (2015) 328–335.
[39] J. Ren, T. Kang, R. Xue, C. Ge, Biosensor based on a glassy carbon electrode modified with tyrosinase immmobilized on multiwalled carbon nanotubes, Microchim. Acta 174 (2011) 303–309.
[40] A.A. Ensafi, B. Saeid, B. Rezaei, A.R. Allafchian, Differential pulse voltammetric determination of methyldopa using MWCNTs modified glassy carbon decorated with $NiFe_2O_4$ nanoparticles, Ionics 21 (2015) 1435–1444.
[41] H. Li, M. Li, W.Y. Shih, P.I. Lelkes, W.H. Shih, Cytotoxicity tests of water soluble ZnS and CdS quantum dots, J. Nanosci. Nanotechnol. 11 (2011) 1–9.